Mechanics of Advanced Composite Structures 5 (2018) 91–102

Semnan University

Mechanics of Advanced Composite Structures

Journal homepage: http://MACS.journals.semnan.ac.ir

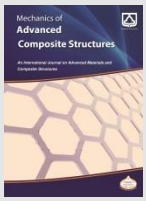

Geometric Effects on Nanopore Creation in Graphene and on the Impact-withstanding Efficiency of Graphene Nanosheets

S. Sadeghzadeh*

Assistant Professor, Head of Smart Micro/Nano Electro Mechanical Systems Lab (SMNEMS Lab), School of New Technologies, Iran University of Science and Technology (IUST), 16846-13114, Tehran, Iran

PAPER INFO

Paper history:
Received 2016-08-15
Revised 2017-07-23
Accepted 2017-09-08

Keywords:
Single-layer Graphene Sheets
Impact-withstanding Efficiency
Nanopore
Withstanding properties
Molecular Dynamics

ABSTRACT

Single- and multilayer graphene sheets (MLGSs) are projectile-resisting materials that can be bombarded by nanoparticles to produce graphene sheets of various sizes and distributions of nanopores. These sheets are used in a variety of applications, including DNA sequencing, water desalination, and phase separation. Here, the impact-withstanding efficiency of graphene nanosheets and the primary factors affecting creation of nanopores in these sheets were studied using a molecular dynamics method. The velocity of impacting nanoparticles and resulting displacement in graphene nanosheets are not sufficient criteria for evaluating the impact resistance of sheets with more than six layers. Instead, visual inspection of the bottom side of a graphene sheet should be used. Self-healing is the most important aspect of MLGSs because it closes the paths of penetrating nanoparticles in the upper layers of the sheets. For nanosheets with few layers, self-healing is observed only at very small nanoparticle velocities; however, when the number of layers is more than six, self-healing occurs even at high nanoparticle velocities. In nanoribbon simulations, it was found that layer boundaries improve resistance against projectile impacts that create well-defined oval shapes. By increasing the distance between layers, the carbon atoms of each layer experience more collisions with the carbon atoms of other layers. Thus, increasing the interlayer distance causes the number of unwanted collisions between carbon atoms to increase and the graphene nanosheets to disintegrate. Additionally, as the circularity of nanopores increases, they become more circular and homogeneous, in turn increasing interlayer spacing, the impact-withstanding efficiency of the sheets, and the circular shape of created nanopores.

1. Introduction

Graphene, a single- or multilayer arrangement of carbon atoms in a honeycomb configuration, is a well-known, two-dimensional material that has opened up new fields of research, led to the development of various nano sensors and actuators, and created new classes of nano electro mechanical systems. Graphene is used in conductive inks, very small-scale transistors, polymer fillers, flexible liquid crystal displays, organic light-emitting diodes, and other applications. Because of its unique combination of exceptional features and properties, graphene is the most promising nanomaterial because of its strong potential for widespread use, especially in applications for which conventional materials are unsuitable.

More research and development is needed before the full potential of graphene can be exploited for practical applications. Apart from its nano-electro-mechanical abilities, graphene has potential for use in sensing applications; for example, the high conductivity and transparency of graphene sheets can be

* Corresponding author. Tel.: +98-21-73225812; Fax: +98-21-73021482
E-mail address: sadeghzadeh@iust.ac.ir

DOI: 10.22075/MACS.2018.1546.1073

used to manufacture transparent electrodes for touch screens [1] and solar cells [2]. This conductivity, alongside large surface areas could also be used in electric batteries [3], optoelectronics [4], and photo catalysts [5]. Some nanocomposite configurations have also been developed to improve the efficiency of graphene-based devices, such as efficient and novel methods of making nano composites by treating graphene nanosheets with vinyl triethoxysilane and successfully blending them with low density polyethylene (LDPE) [6].

Multilayer graphene sheets (MLGSs) can also be used as projectile-resisting materials, especially since preparation of such sheets is simple [7]. This has facilitated implementation of graphene sheets in ballistic applications; however, new concepts should be developed to obtain low-cost and sufficiently strong graphene-based protective barriers, for which computational studies are suggested rather than expensive experimentation. However, several nano indentation experiments have been performed to investigate the tensile and mechanical properties of graphene sheets. One experiment involved a low-speed test (<< 1 m/s) with strain rates reaching ~105–106 1/s for very thin samples [8]. Most high-speed, high-strain-rate mechanical characterization techniques, such as the split Hopkinson pressure bar [9] and ballistic tests [10], are inappropriate for testing very thin specimens [11].

One significant study employed the ion bombardment process to investigate ion implantation and irradiation of graphene to understand the material's behavior in irradiative environments. It was found that large incident angles are necessary for substitution of especial nanopores and producing single vacancies, while smaller incident angles are appropriate for forming double vacancies, multiple vacancies, and in-plane disorders [12, 13]. In another study, the bombardment of a suspended monolayer graphene sheet by different energetic atoms was explored using the classical molecular dynamics approach and a reactive force field (i.e., ReaxFF) [14]. This study found that the number, shape, size, and distribution of defects were primarily determined by the impact site, properties of the impacting atoms, and the incident energy.

By combining ion beam experiments and atomistic simulations, the production of defects in graphene on Ir(111) substrate by low-energy Xe ions at grazing incidence was also investigated [15]. This research demonstrated that bombarding ions are channeled in between the graphene and substrate, creating chains of vacancy clusters with edges bent down toward the substrate. In [16], the normal and tangential coefficients of restitution for gaseous molecules colliding layer-wise with single-layer and MLGSs were calculated using the non-equilibrium molecular dynamics method. These depended on the impact angle, velocity, and landing position of projectiles, and parameters were evaluated computationally by implementing several operations. In [17], a quasi-classical model for the collision of various nanoparticles with single- and few-layer graphene nanosheets was introduced as a multi-scale approach that coupled non-equilibrium molecular dynamics with the finite element method. It was observed that the coefficient of restitution and the induced stresses depended on the impact velocity of the projectiles. In [18], the penetration-resistance efficiency of single- and MLGSs was investigated by employing the multiscale approach, concentrating on optimal spacing between graphene layers to improve the impact properties of graphene sheets as important candidates for novel impact-resistant panels. There are also some valuable works on the advanced application of graphene sheets [19-21].

In this paper, the molecular dynamics method was employed to investigate the effects of geometric parameters on the resistance of graphene nanosheets against nanoparticle impact. In studying the impact-withstanding strength of MLGSs and the creation of nanopores within them, the number of layers was an important parameter for optimizing the efficiency of graphene nanosheets.

2. Withstanding Projectile Impact: A Fascinating Feature of Graphene Nanosheets

Figure 1 shows the general configuration of nanoparticles bombarding a MLGS. Owing to its remarkable mechanical properties, graphene can reliably withstand the impact of high-speed nanoparticles.

3. Producing Nanopores in Graphene: A Fascinating Concept

There are several techniques, such as ion beam irradiation, for fabricating nanoporous graphene for various applications, including DNA sequencing, water desalination, and phase separation [13, 22]. All applications require efficient fabrication of nanoporous graphene using a highly-controlled process. The bombardment of graphene by argon gas and gold clusters is a promising method for creating porous graphene; however, in practice, such experiments are challenging to perform due to the difficulty of producing gas and metal clusters [13, 22].

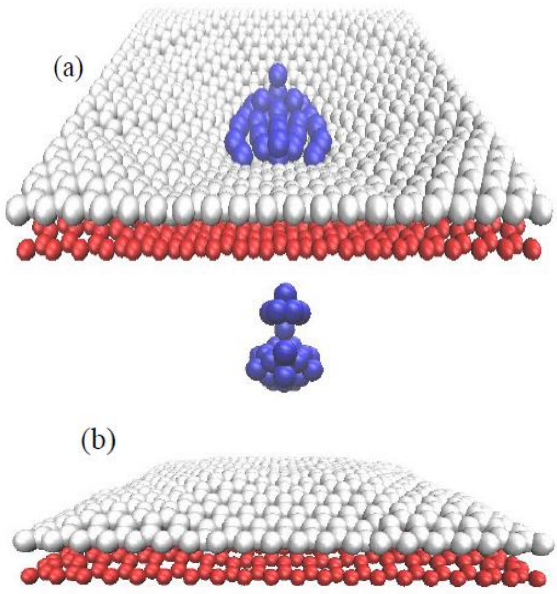

Figure 1. General configuration of nanoparticles bombarding a MLGS; (a) before collision, (b) after collision and rebound from the graphene sheet

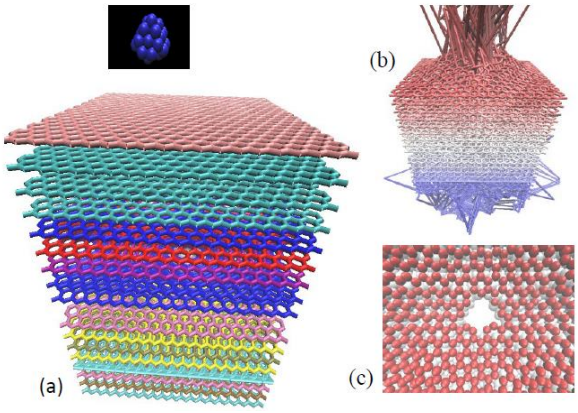

Figure 2. General schematics of a nanoparticle cluster thrown onto a graphene reinforced microplate

Assuming that the mechanical strength of a MLGS is only provided by graphene layers, Figure 2(b) shows the ruptured bonds of carbon atoms in a MLGS. The ruptured structure is rough and no pores are created. In contrast, an approximately circular hole is created in a two-layer graphene sheet (2LG) by bombarding it with a high-speed nanoparticle cluster.

4. Model

Molecular dynamics integrates the discrete equations of motion, which are derived as

$$m_i \ddot{u}_i = -\nabla_i U(u_1 : u_N), \quad (1)$$

where m_i, u_i, and $U(u_1 : u_N)$ denote the mass, displacement, and interatomic potential, respectively, for each N atom. Here, the Tersoff potential [23] was used for the interaction between carbon atoms, and the pair coefficients were chosen from [23]. For the interfacial force field (i.e., graphene–graphene and graphene–metallic nanoparticles), the Lennard–Jones potential was implemented, and the depth of potential well (ε [eV]) and the finite distance at which the inter-particle potential was zero (σ[°A]) were obtained from the Lorentz–Berthelot mixing rule ($\varepsilon_{ij} = \sqrt{\varepsilon_{ii}\varepsilon_{jj}}$ and $\sigma_{ij} = \frac{1}{2}[\sigma_{ii} + \sigma_{jj}]$).

5. Results and Discussion

5.1. Effect of the number of layers

5.1.1. Fewer layers of graphene are more efficient

Figure 3 shows the deformation of single-layer graphene (SLG) and 2LG sheets impacted by steel nano projectiles. More projectile energy is absorbed as the number of layers increases; however, comparison between the specific critical rupture velocities $\mathbf{V^*} = \frac{\mathbf{V_{cr}}}{\mathbf{M}}$ (defined as the critical rupture velocity at which a sheet is perforated divided by the MLGS mass) shows that fewer layers of graphene have better impact resistance efficiency. Thus, for the same weight, a serial configuration of fewer layers is more efficient for withstanding projectile impact compared to MLGS with a larger number of layers.

Table 1. Coefficients of the Lennard–Jones potential for various interfaces [24, 25]

Elements	C-Fe	Au-Au	C-Au	C-C
ε (eV)	0.0409	0.22747	0.022	0.00239
σ (°A)	2.9635	2.737	2.74	3.41

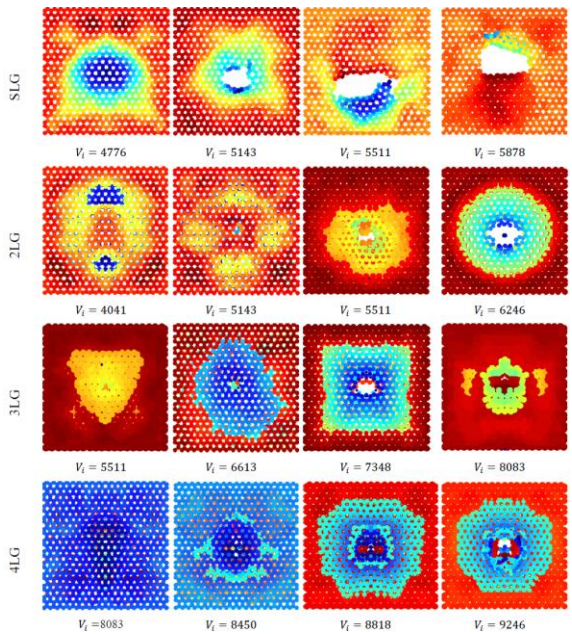

Figure 3. Rupture of single to four-layer graphene (4LG) plates due to the impact of a projectile moving at subcritical and supercritical velocities

5.1.2. Interpreting the findings

5.1.2.1. Velocity and displacement of nanoparticles

Figure 4 shows the vertical displacement and the velocity of a nanoparticle before, during, and after collision with SLG, 2LG, and three-layer graphene (3LG) sheets. The displacement and velocity diagrams both indicate the rupture of graphene sheets and the passing of nanoparticles that moved with a constant acceleration, caused by the constant force applied, and reached considerable velocities before colliding with the graphene sheets. After the nanoparticles collided with the graphene sheets, they either rebounded from or penetrated the surface. These actions were determined by the sign of the nanoparticle's velocity after collision. Figure 4 shows that a nanoparticle's velocity after impact remained negative only at certain initial speeds, indicating nanoparticles that passed through the sheets. A positive final velocity indicated that a nanoparticle had rebounded from a sheet and had moving upward. The same conclusions could be reached by analyzing the displacement diagrams.

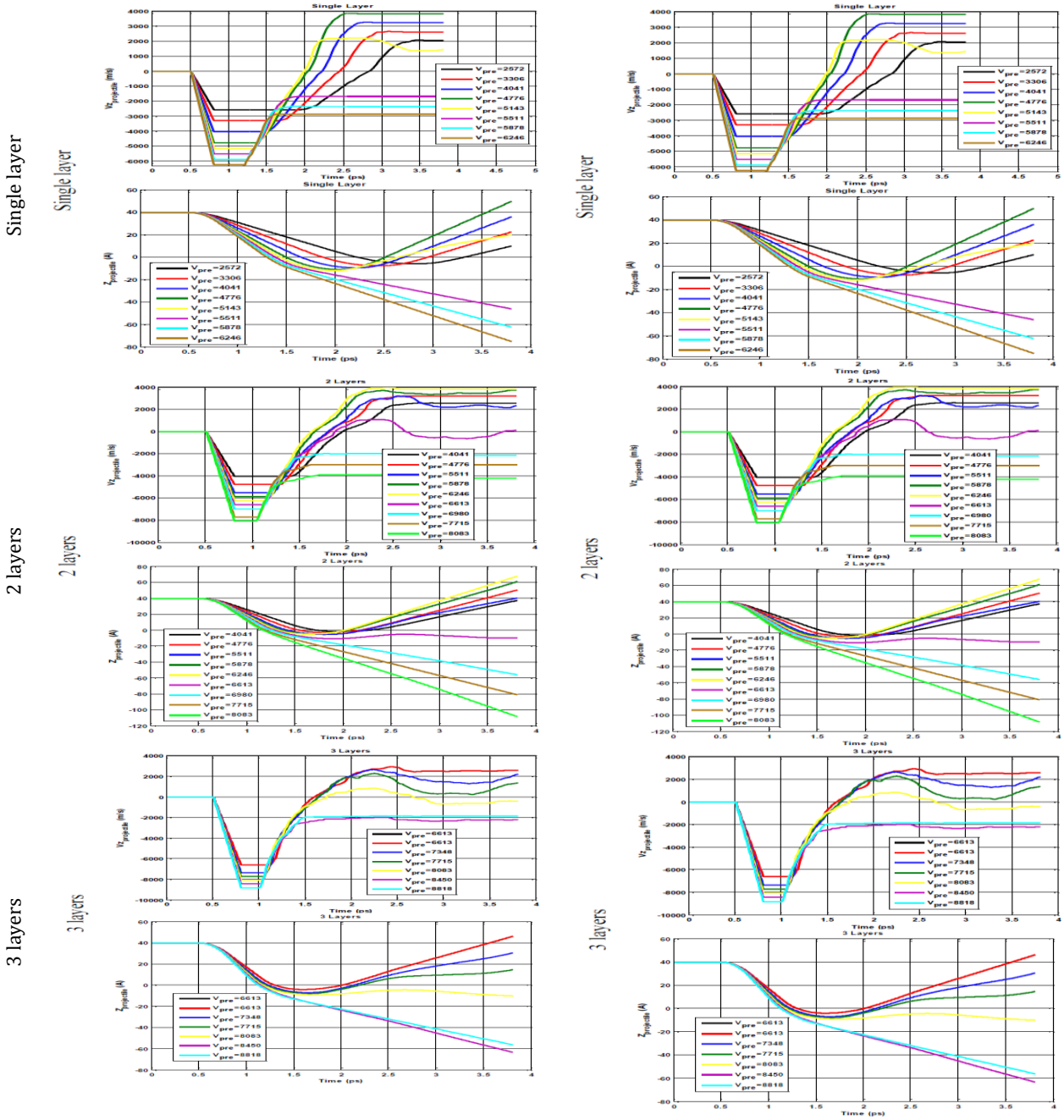

Figure 4. Vertical displacement and velocity of nanoparticle before, during, and after collision with SLG, 2LG, and 3LG sheets

When a nanoparticle rebounded from a graphene sheet, it moved upward, and the vertical distance from the sheet increased substantially. In contrast, when a nanoparticle passed through the graphene sheet, its vertical distance from the sheet gradually diminished. This trend was observed only for SLG, 2LG, and 3LG sheets, and when more layers were present, neither the vertical velocity diagrams nor the displacement diagrams showed the rebounding of nanoparticles.

Figure 5 shows the same diagrams for 4LG, five-layer graphene (5LG), and six-layer graphene (6LG) sheets. Although some final velocities are positive and some diagrams show an increase in displacement following a collision, the penetration of graphene sheets occured at lower velocities. Thus, velocity and displacement parameters are not appropriate criteria for predicting the final shape of graphene sheets.

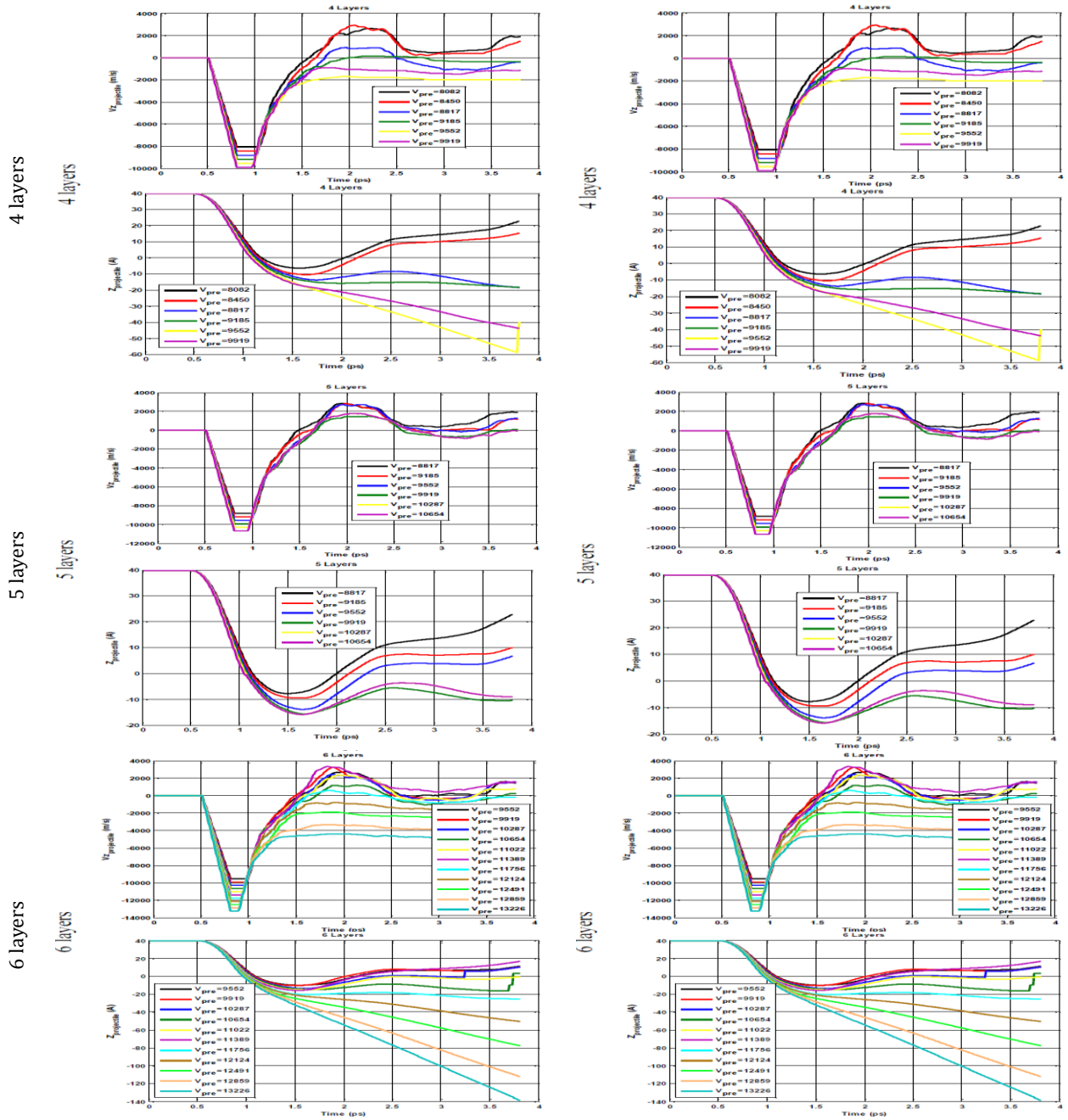

Figure 5. Vertical displacement and velocity of nanoparticle before, during, and after collision with 4LG, 5LG, and 6LG sheets

The results become more inappropriate as the number of layers increased. Figure 6 shows the vertical velocities and displacements of nanoprojectiles for ten-layer graphene (10LG) and 20-layer graphene (20LG) sheets. As these diagrams indicate based on vertical velocity and displacement criteria, there should be no rupture in the sheets; however, a rupture occurred.

5.1.2.2. Visual inspection of nanosheets

It is suggested that visual inspection of the final shape of graphene sheets is a more suitable criterion. Figure 7 depicts the initial configuration, top view, and bottom view of SLG, 2LG, and 3LG sheets. By checking both the top and the bottom views, the rupture of graphene sheets with fewer layers due to the penetration of nanoparticles can be ascertained more reliably.

Figure 8 shows the same views for 4LG, 5LG, and 6LG sheets. Although the bottom view illustrates the sheet rupture, it is very difficult to recognize the actual rupture of the sheet because of the almost intact top side.

The recognition of sheet penetration and rupture becomes even more challenging when the number of layers increases. Figure 9 depicts the initial configuration, top view, and bottom view of 10-layer and 20-layer graphene sheets. Although the top side of each sheet is completely intact, the bottom view shows a penetrated graphene sheet.

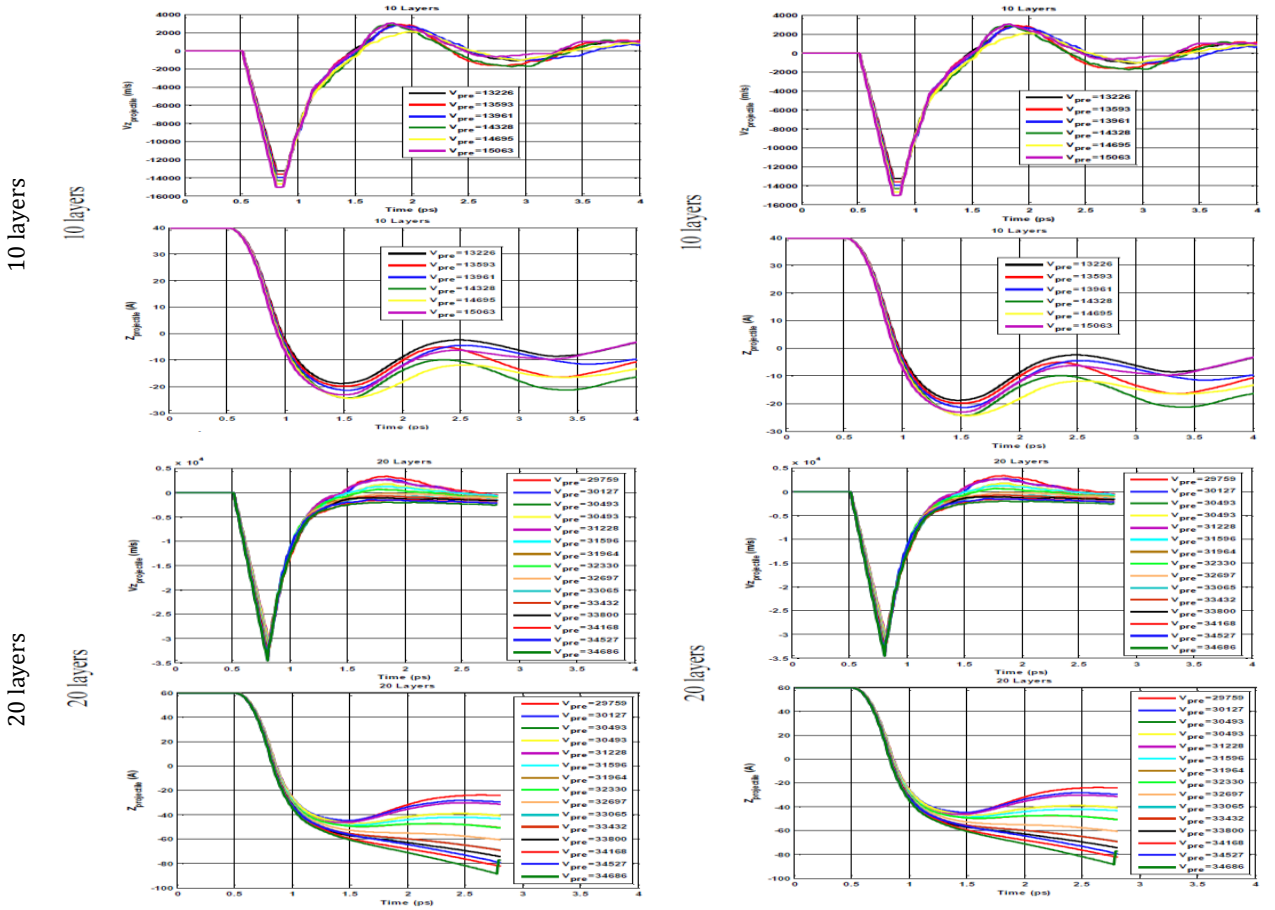

Figure 6. Vertical displacement and velocity of nanoparticle before, during, and after collision with 10LG and 20LG sheets

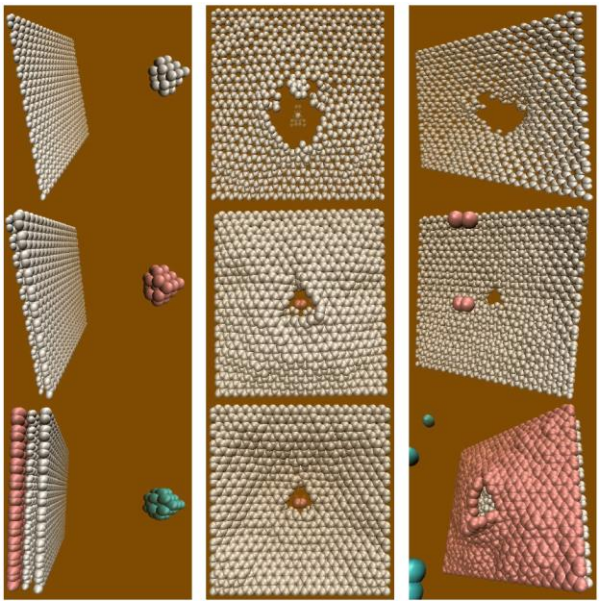

Figure 7. Initial configuration, top view, and bottom view of SLG, 2LG, and 3LG sheets

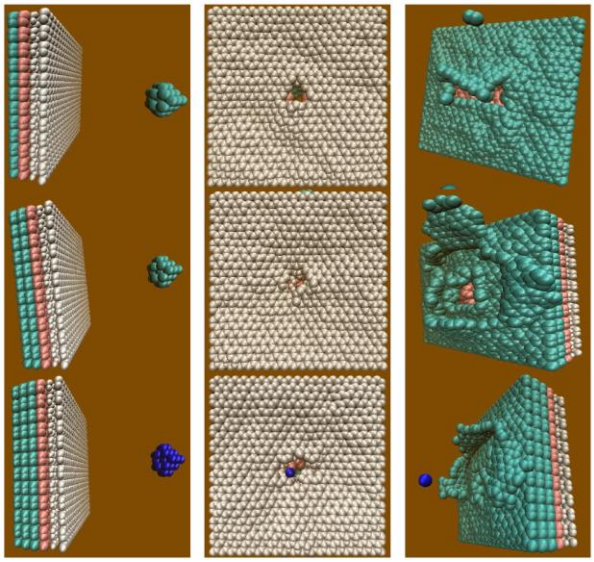

Figure 8. Initial configuration, top view, and bottom view of 4LG, 5LG, and 6LG sheets

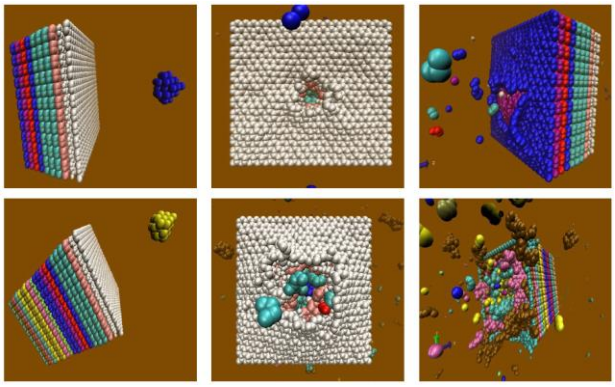

Figure 9. Initial configuration, top view, and bottom view of 10LG and 20LG sheets

Self-healing is the most important dynamic observed in MLGSs, resulting from the closing of the nanoparticle path in the upper layers of the sheet. For graphene sheets with fewer layers, self-healing is only observed at very small nanoprojectile velocities, while for sheets with more than six layers, self-healing occurs even at high nanoparticle velocities. During the self-healing process, there is a specific time window that allows the observation of a complete hole in a sheet before carbon atoms begin to bond with neighboring atoms and self-healing begins. Figure 10 shows the top view of an imperfectly self-healed, 4LG sheet in 2.11 ps.

Increasing the number of layers helps the self-healing of MLGSs. Distributing the imposed stress among more layers decreases the separation of carbon atoms and leads to better self-healing. Figure 11 shows a complete hole in a 5LG sheet at 1.89 ps and the perfect self-healing of the nanosheet after 4 ps.

Figure 12 depicts a complete hole in a 6LG sheet at 2.32 ps and the perfect self-healing of the nanosheet after 4 ps.

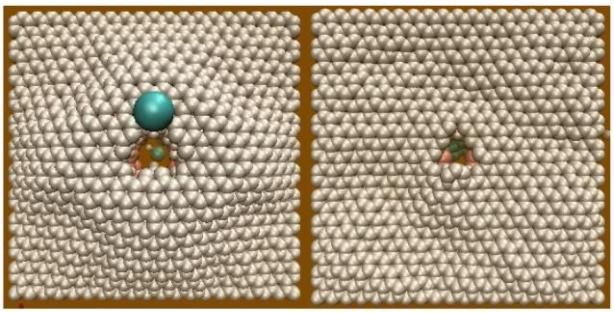

Figure 10. Top views showing a complete hole in a 4LG sheet at 2.11 ps (left) and the imperfect self-healing of the nanosheet after 4 ps (right)

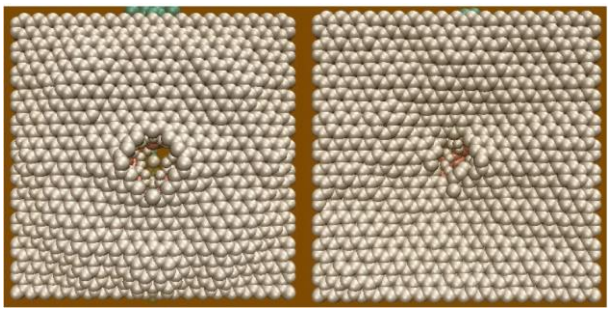

Figure 11. Top views showing a complete hole in a 5LG sheet at 1.89 ps (left) and the perfect self-healing of nanosheet after 4 ps (right)

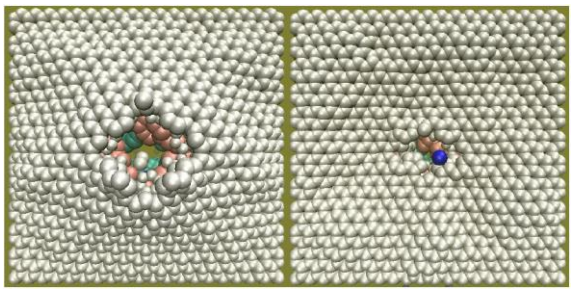

Figure 12. Top views showing a complete hole in a 6LG sheet at 1.89 ps (left) and the perfect self-healing of nanosheet after 4 ps (right)

Figure 13 shows the critical rupture velocities for SLG to 20LG sheets. The critical rupture velocity increases linearly with the increase in the number of sheet layers. However, the specific critical rupture velocity decreases asymptotically as the number of layers increases. Thus, an array of fewer graphene layers can withstand much higher projectile impact velocities than an MLGS of equivalent weight with more layers. This can be used to optimize and tradeoff between various parameters of protective graphene-based barriers. According Figure 13, the capacity of an SLG sheet for withstanding the impact of a projectile is 3.64 times that of a 20LG sheet; thus, twenty graphene layers spaced at least several nanometers apart and using the usual polymeric barriers (i.e., non-interacting graphene layers) allow a critical rupture velocity to be achieved that is 3.64 times that of an ordinary 20LG sheet.

5.2. Effect of the sheet aspect ratio

Defining the aspect ratio of graphene sheets as ($AR = \frac{L_x}{L_y}$), the most significant discrepancy between sheet performance is observed for AR = 2 for all simulations. The low levels of energy dissipation in sheet configurations with fewer layers (0.09%, 0.57%, 1.8%, and 2.31% and 2.89% for single-layer to 4LG sheets) indicate the minimal influence of the aspect ratio.

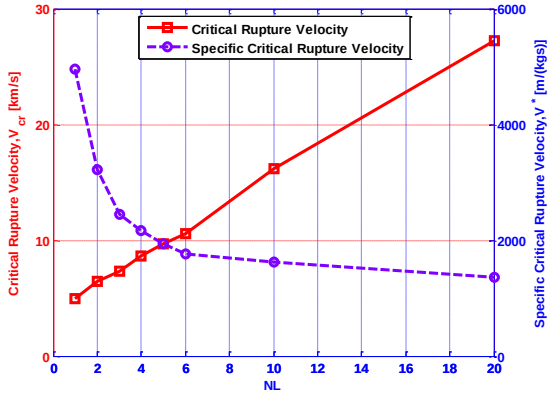

Figure 13. Critical and specific critical rupture velocities for SLG to 20LG sheets versus the number of layers

A considerable difference is reported for sheets with more layers, for which the maximum projectile energy dissipation occurs at AR = 2 and energy losses of 6.35%, 9.12%, and 21.16% for 6LG, 10LG, and 20LG sheets, respectively, emphasize the influence of the aspect ratio on the impact resistance efficiency of thicker sheets. Details are given in Table 2.

Figure 14 depicts all five cases related to different aspect ratios. In the first case, a nanoribbon is simulated and the boundaries have a substantial effect on increasing impact resistance. The hole created by the impact has a well-defined oval shape; thus, the aspect ratio is very important to producing nanopores of desired shapes but is not effective for improving impact-withstanding efficiency. By bringing the size of a graphene sheet's width closer to its length, the holes produced by impact tend to be more circular in shape.

5.3. Effect of interlayer distance

The influence of interlayer distance on ballistic performance has been investigated for various barrier materials, such as fabrics [26]. On large scales, fabric and metal barriers can be arranged in a serial array to offer more resistance to projectile impact. However, this requires more space and considerably increases the weight of the barrier. On small scales, interlayer interactions, when the distance between two adjacent layers of graphene is increased to more than the common interplay distance of the MLGSs (3.35 Å), interactions are weakened and the prepared MLGS becomes several SLG sheets in a parallel configuration. Since the energy loss of a projectile in a 2LG sheet is lower than twice the energy loss in a SLG sheet, by spacing several SLG sheets, higher projectile velocities and masses can be resisted with the same barrier weight, while keeping the barrier thickness thin and overall dimensions in acceptable ranges.

Table 2. Effect of the aspect ratio of SLG and 4LG sheets on projectile energy loss

AR	L_x(nm)	L_y(nm)	1L		4L	
			V_{impact}	ΔE (%)	V_{impact}	ΔE (%)
1	3	3	67,372	0	351,891	0
2	4.2426	2.1213	67,348	0.13	351,001	2.73
3	5.1962	1.7321	67,359	0.058	351,543	2.05
4	6	1.5	67,382	0.035	351,502	2.81
5	6.7082	1.3416	67,355	0.098	351,725	1.57

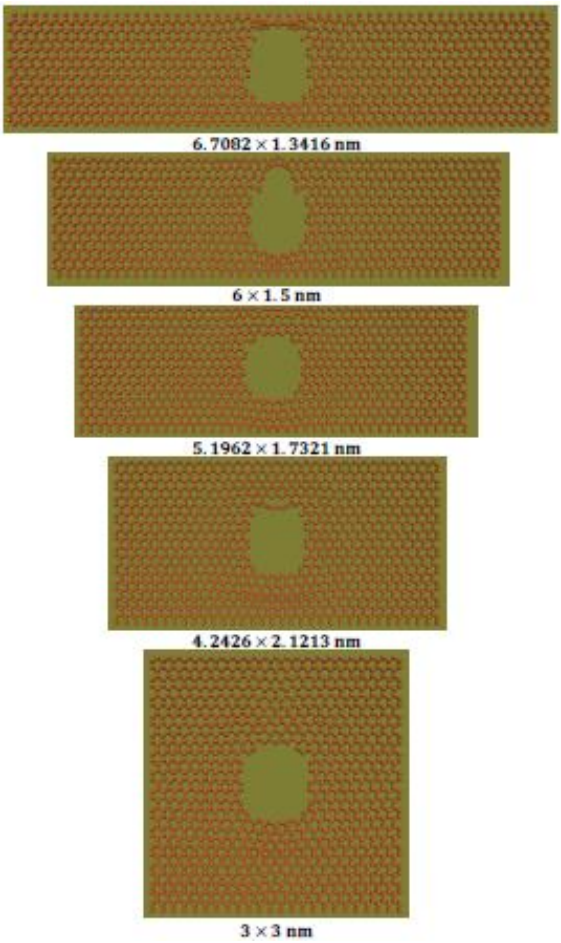

Figure 14. Nanopores created by shooting a high-speed bullet onto graphene sheets of various aspect ratios

Figure 15 shows the velocity losses of a projectile passing through a 2LG sheet with various dimensionless interlayer distances. The non-dimensional interlayer distance is defined as

$$\delta = \frac{layers\ distance}{\delta_0}, \qquad (2)$$

where $\boldsymbol{\delta_0}$ is the common interlayer distance for MLGSs ($\boldsymbol{\delta_0 = 3.35\ °A}$).

Table 3 lists the impact and residual velocities and energy losses for 2LG and 4LG sheets with various interlayer distances. A pronounced increase in energy loss is observed when the distance between layers increases; however, the difference diminishes at larger interlayer distances.

Figure 16 depicts the specific penetration energy for spaced 2LG and 4LG sheets versus the dimensionless interlayer spacing (δ). For both cases, it is observed that the specific penetration energy increases with the increase of interlayer spacing and that, for the 2LG sheet, the specific penetration energy increases asymptotically with the increase of the dimensionless distance between layers.

Although the specific penetration energy results indicate that the impact-withstanding properties of MLGSs improve with the increase in interlayer distance, the sheets are disintegrated more severely as the spacing between layers increases. The top row of Figure 17 shows that, with increased interlayer distance, carbon atoms in different layers experience more collisions with carbon atoms in other layers. Thus, by increasing the distance between layers, the number of unwanted collisions between atoms increases and the disintegration of layers becomes more severe.

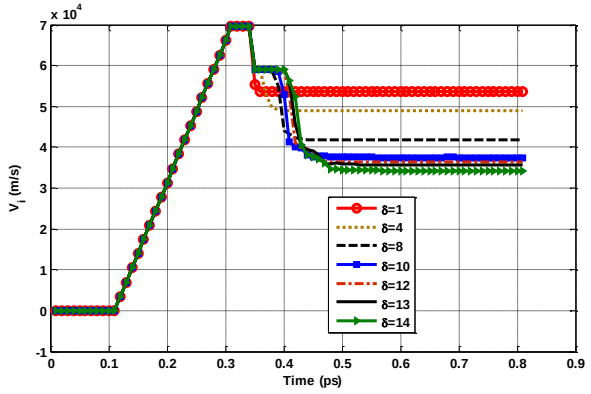

Figure 15. Velocity loss of a projectile passing through a 2LG sheet with various dimensionless interlayer distances δ

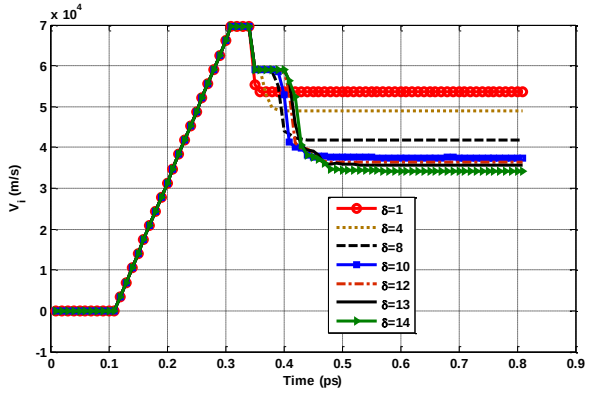

Figure 16. Specific penetration energy for spaced 2LG and 4LG sheets versus dimensionless interlayer spacing

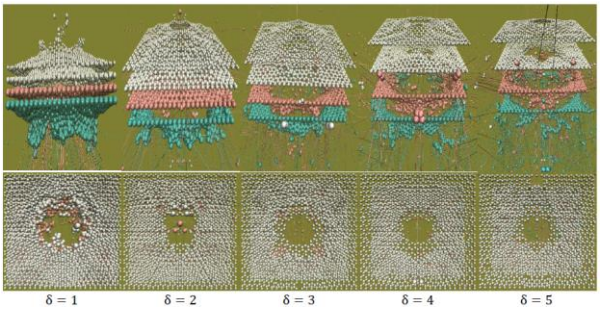

Figure 17. Increased disintegration of MLGSs and increased circularity of produced holes due to increased interlayer distance

Table 3. Comparing the energy losses in 2LG and 4LG sheets with various distances between their layers

δ	2 lay				4 lay			
	V_{impact}	$V_{residual}$	E^*_{Loss}	ΔE (%)	V_{impact}	$V_{residual}$	E^*_{Loss}	ΔE (%)
1	69,581.24	53,529.08	0.4082	0	52,168.3196	30,189.1410	0.6651	0
2	69,581.09	50,371.21	0.4759	16.6	52,168.3196	23,129.6298	0.8034	20.79
3	69,581.21	51,121.55	0.4602	12.74	52,168.3196	22,787.0977	0.8092	21.66
4	69,581.21	48,861.01	0.5069	24.18	52,168.3196	17,874.7021	0.8826	32.69
5	69,581.21	49,315.34	0.4977	21.92				
6	69,581.21	44,010.05	0.5999	46.98				
7	69,581.21	45,173.32	0.5785	41.73				
8	69,581.21	41,903.75	0.6373	56.14				
9	69,581.21	39,294.22	0.6811	66.86				
10	69,581.21	37,466.24	0.7101	73.96				
11	69,581.21	36,179.17	0.7296	78.75				
12	69,581.21	36,325.09	0.7275	78.22				
13	69,581.21	35,688.13	0.7369	80.54				
14	69,581.21	34,249.46	0.7577	85.63				

The produced nanopores become more circular and homogeneous as the interlayer distance increases. The bottom row of Figure 17 clearly demonstrates this behavior. Therefore, by spacing the graphene layers further apart, the impact-withstanding efficiency of graphene sheets is improved and the created nanopores become more circular, which was the purpose of this research.

6. Conclusion

For designing proper barriers to withstand the impact of high-speed projectiles and to create desired nanopores in graphene nanosheets for special applications, the molecular dynamics approach was employed to study the effects of certain parameters, such as the number of layers, sheet aspect ratio, and interlayer distance on the impact-withstanding efficiency of graphene sheets. It was demonstrated that the velocity and displacement of impacting nanoparticles are not sufficient criteria for evaluating the impact-withstanding efficiency of graphene nanosheets with more than six layers and that visual inspection of the bottom side of a graphene sheet is a better method for this purpose.

Self-healing was the most important feature of MLGSs and closed the path of passing nanoparticles in the upper layers of the nanosheets. For nanosheets with few layers, self-healing was observed only at very small nanoparticle velocities; however, when the number of layers was more than six, self-healing behavior was observed even at high nanoparticle velocities.

Critical rupture velocity increases linearly with the increase in the number of layers. However, the specific critical rupture velocity decreases asymptotically as the number of layers increases. Thus, a large-scale array of fewer graphene layers can withstand much higher projectile impact velocities than an MLGS of equivalent weight with more layers. Thus, using 20LGs that are spaced at least several nanometers apart and including the usual polymeric barriers (i.e., no graphene layer interaction), a critical rupture velocity can be achieved that is 3.64 times that of an ordinary 20LG sheet.

By studying the effects of sheet aspect ratio, the most significant discrepancy between the performances of graphene sheets was observed when AR = 2 rather 1, for all simulations. The low levels of energy loss in graphene sheet configurations with few layers indicate the minimal effect of the aspect ratio, while considerable difference in impact resistance was observed for multilayer nanosheets with more layers. In the nanoribbon simulation, boundaries had a significant effect and helped the nanoribbon resist impact; additionally, the penetration holes produced in nanoribbons were of a well-defined oval shape

In evaluating the interlayer distance effect, it was discovered that because projectile energy loss in 2LG sheets is lower than twice the energy loss in SLG sheets, by spacing several SLG sheets, higher projectile velocities and masses can be resisted with the

same barrier weight, while keeping the barrier thickness thin and overall dimensions in acceptable ranges. The specific penetration energy of MLGSs increases asymptotically with the increase in dimensionless spacing between layers. Although specific penetration energy results indicate that the impact-withstanding properties of MLGSs improve with the increase in interlayer distance, the sheets disintegrate more severely as the spacing between layers increases because carbon atoms experience more collisions with the carbon atoms in other layers. Additionally, the produced nanopores become more circular and homogeneous as the interlayer distance increases. Therefore, by increasing the interlayer spacing, the impact-withstanding efficiency of graphene sheets against projectile impact is improved and the created nanopores become more circular in shape.

The best conditions for creating circular nanopores are:

- Decreasing the number of layers,
- Increasing the aspect ratio of the sheet, and
- Increasing interlayer spacing.

References

[1] Bae S, Kim H, Lee Y, Xu X, Park J-S, Zheng Y, Balakrishnan J, Lei T, Kim HR, Song YI. Roll-to-roll production of 30-inch graphene films for transparent electrodes. *Nature nanotechnology* 2010; 5(8): 574.

[2] Bonaccorso F, Sun Z, Hasan T, Ferrari A. Graphene photonics and optoelectronics. *Nature photonics* 2010; 4(9): 611.

[3] Zhou G, Paek E, Hwang GS, Manthiram A. Long-life Li/polysulphide batteries with high sulphur loading enabled by lightweight three-dimensional nitrogen/sulphur-codoped graphene sponge. *Nature communications* 2015; 6: 7760.

[4] Kim YD, Kim H, Cho Y, Ryoo JH, Park C-H, Kim P, Kim YS, Lee S, Li Y, Park S-N. Bright visible light emission from graphene. *Nature nanotechnology* 2015; 10(8): 676.

[5] Bo W, Liu Z, Hong T, Han J, Guo K, Zhang X, Chen D. Trilaminar graphene/tremella-like CuInS 2/graphene oxide nanofilms and the enhanced activity for photoelectrochemical water splitting. *J. Nanopart. Res.* 2015; 17(7): 295.

[6] Wang J, Xu C, Hu H, Wan L, Chen R, Zheng H, Liu F, Zhang M, Shang X, Wang X. Synthesis, mechanical, and barrier properties of LDPE/graphene nanocomposites using vinyl triethoxysilane as a coupling agent. *J. Nanopart. Res.* 2011; 13(2): 869-78.

[7] Sidorov AN, Yazdanpanah MM, Jalilian R, Ouseph P, Cohn R, Sumanasekera G. Electrostatic deposition of graphene. *Nanotechnology* 2007; 18(13): 135301.

[8] Gotsmann B, Rothuizen H, Duerig U. Ballistic nanoindentation of polymers. *Appl. Phys. Lett.* 2008; 93(9): 093116.

[9] Gama BA, Lopatnikov SL, Gillespie JW. Hopkinson bar experimental technique: a critical review. *Applied mechanics reviews* 2004; 57(4): 223-50.

[10] Zukas JA. **High velocity impact dynamics**. Wiley-Interscience; 1990.

[11] Lee J-H, Loya PE, Lou J, Thomas EL. Dynamic mechanical behavior of multilayer graphene via supersonic projectile penetration. *Science* 2014; 346(6213): 1092-6.

[12] Bai Z, Zhang L, Liu L. Bombarding graphene with oxygen ions: combining effects of incident angle and ion energy to control defect generation. *The Journal of Physical Chemistry C* 2015; 119(47): 26793-802.

[13] Bai Z, Zhang L, Liu L. Improving low-energy boron/nitrogen ion implantation in graphene by ion bombardment at oblique angles. *Nanoscale* 2016; 8(16): 8761-72.

[14] Liu XY, Wang FC, Park HS, Wu HA. Defecting controllability of bombarding graphene with different energetic atoms via reactive force field model. *J. Appl. Phys.* 2013; 114(5): 054313.

[15] Standop S, Lehtinen O, Herbig C, Lewes-Malandrakis G, Craes F, Kotakoski J, Michely T, Krasheninnikov AV, Busse C. Ion impacts on graphene/Ir (111): interface channeling, vacancy funnels, and a nanomesh. *Nano Lett.* 2013; 13(5): 1948-55.

[16] Sadeghzadeh S. On the oblique collision of gaseous molecules with graphene nanosheets. *Molecular Simulation* 2016; 42(15): 1233-41.

[17] Sadeghzadeh S, Liu L. Resistance and rupture analysis of single-and few-layer graphene nanosheets impacted by various projectiles. *Superlattices Microstruct.* 2016; 97: 617-29.

[18] Sadeghzadeh S. Benchmarking the penetration-resistance efficiency of multilayer graphene sheets due to spacing the graphene layers. *Appl. Phys. A* 2016; 122(7): 655.

[19] Sadeghzadeh S, Rezapour N. The mechanical design of graphene nanodiodes and nanotransistors: geometry, temperature and strain effects. *RSC Advances* 2016; 6(89): 86324-33.

[20] Sadeghzadeh S, Rezapour N. A study of thermal conductivity in graphene diodes and transistors with intrinsic defects and subjected to metal impurities. *Superlattices Microstruct.* 2016; 100: 97-111.

[21] Sadeghzadeh S. Computational design of graphene sheets for withstanding the impact of ultrafast projectiles. *J. Mol. Graphics Modell.* 2016; 70: 196-211.
[22] Bai Z, Zhang L, Liu L. Bombarding graphene with oxygen ions: combining effects of incident angle and ion energy to control defect generation. *The Journal of Physical Chemistry C* 2015; 119(47): 26793-802.
[23] Tersoff J. Modeling solid-state chemistry: Interatomic potentials for multicomponent systems. *Physical Review B* 1989; 39(8): 5566.
[24] Heinz H, Vaia R, Farmer B, Naik R. Accurate simulation of surfaces and interfaces of face-centered cubic metals using 12– 6 and 9– 6 Lennard-Jones potentials. *The Journal of Physical Chemistry C* 2008; 112(44): 17281-90.
[25] Hirschfelder J, Bird RB, Curtiss CF. **Molecular theory of gases and liquids**. 1964.
[26] Lim C, Tan V, Cheong C. Perforation of high-strength double-ply fabric system by varying shaped projectiles. *International Journal of Impact Engineering* 2002; 27(6): 577-91.